Applied Acoustics 161 (2020) 107190

Contents lists available at ScienceDirect

Applied Acoustics

journal homepage: www.elsevier.com/locate/apacoust

Sound radiation of hollow box timber floors under impact excitation: An experimental parameter study

Simone Conta [a,*], Anders Homb [a,b]

[a] NTNU, Department of Civil and Environmental Engineering, 7491 Trondheim, Norway
[b] SINTEF Community, 7465 Trondheim, Norway

ARTICLE INFO

Article history:
Received 17 September 2019
Received in revised form 12 November 2019
Accepted 16 December 2019

Keywords:
Timber hollow-box floor
Experimental modal analysis
Integral transform method
Radiated sound power
Impact noise level

ABSTRACT

The timber building industry is developing building systems for urban buildings with open architecture based on long span floor systems. Span length can be increased with constant cross section by combining stiff floor elements e.g. hollow-box floors with supports that provide high rotational stiffness. Detailed knowledge of the vibroacoustic behavior of such a system is not available and is needed to design buildings that fulfill the requirements in an economic and sustainable way. We set up a prototype and performed experimental investigations to identify the modal properties of such a system and to gain understanding of the sound radiation properties under impact excitation. The measurements were performed in an industrial hall using experimental modal analysis (EMA) and the Integral Transform method (ITM). The results highlight the limitation of standard acoustic laboratories and show the importance of using advance measurement methods to acquire reliable data. The size of the element and the boundary condition clearly affect the radiated sound power at low frequencies. Sound radiation can be efficiently reduced above 50 Hz by using traditional strategies such as gravel in the cavity of the floor elements. Additionally, insights about the ITM are presented, showing that symmetry cannot be exploited and that there is no requirement for a baffle when impact excitation is under investigation.

1. Introduction

Hollow core slabs are popular when long span is required and are widely used in urban buildings with the most different purposes, including commercial, office and apartment buildings. The timber building industry is developing hollow box floor systems to offer an alternative to hollow core concrete slabs. Development seems to be driven by structural requirements and little literature is available on the acoustic properties [1–3]. More detailed knowledge is crucial if acoustic requirements shall be fulfilled in an efficient and sustainable way in a building typology that is increasingly important in our ever growing and more dense cities.

Hollow box timber floors can reach long span at competitive floor height and with efficient material consumption compared with for instance massive CLT timber floors [4–5]. In order to fulfil acoustic requirements, the hollow volume of these floor elements can be used either to integrate acoustic materials as for example absorbing materials (mineral fibres), additional mass (gravel, concrete) or to install more advanced elements such as mass tuned damper. Several large companies (e.g. Lignatur, StoraEnso [6], MetsäWood [7], Moelven) designed their own products in this category and carried out the development of these floor systems, but there is a lack of public acoustic knowledge and literature on this subject.

Malo [8] showed that stiff end restraints can be exploited to achieve longer span with constant cross section. This has clear structural and economic advantages, but the acoustic implications were not investigated before.

The Norwegian research project WOODSOL aims at developing mid-rise timber buildings (up to 10 stories), based on stiff hollow box floor elements combined with moment resting frames [9] and offers a chance to deepen the knowledge on this subject. The floor elements are hollow boxes partly filled with gravel resulting in a strongly inhomogeneous object, featuring a heavily damped plate on the bottom and a lightly damped plate on the top. The floor elements are combined with a connection system that aims at being moment resisting. The connectors are mounted at the corner of the floor element, giving, in principle, a clamped fixation of the corners.

This results in unique boundary conditions for the sound radiation of the floor elements, which need to be investigated for under-

* Corresponding author at: Institutt for konstruksjonsteknikk, NTNU, Richard Birkelands vei 1A, 7491 Trondheim, Norway.
E-mail address: Simone.Conta@ntnu.no (S. Conta).

https://doi.org/10.1016/j.apacoust.2019.107190
0003-682X/

standing the acoustical behaviour of the structure and – in a second step – serve as basis for the computational models. To accomplish this purpose, we set up an extensive experimental campaign on a prototype of the system.

The main goals of the campaign were: 1) investigate the modal properties of the floor element, 2) investigate the sound radiation properties of the floor element, 3) identify governing factors and possibility to improve impact sound insulation (e.g. stiffness, additional mass), 4) investigate the vibration transmission between floor elements and columns and 5) determine the influence of the connecting detail between floor elements. In this paper, we focus on the experimental investigation, presenting the adopted measurement methods and the results related to the floor elements sound radiation properties (items 1 and 2).

We investigated the sound radiation focusing on impact sound at low frequencies, expecting here the main challenges due to the long span and lightweight properties of the floor elements. Due to the size of the elements, the interest in the specific mounting system and the frequency range of interest, we could not perform ordinary laboratory measurements in a standard acoustic floor test facility. We therefore used two methods to investigate the vibroacoustic properties of our setup; 1) an experimental modal analysis (EMA) to study the modal behaviour and 2) the measurement method denominated *Integral transform method (ITM)* to study the radiated sound power. Various methods are then available to calculate the impact noise level from the radiated sound power (see section 5). We wanted to gather measurement data that eventually allow the comparison of the acoustic performance of the floor element (i.e. the impact noise level L_n) with other documented construction available in literature or common in the practice. This led to the choice of a tapping machine as excitation source and the selection of excitation positions according to the standard ISO16283 [10]. For the data presented in this paper, the frequency range was set from 20 Hz to 400 Hz. The upper frequency limit was chosen considering the requirement of the ITM method (see section 3.2.2.2), its implications in terms of time resources and a reasonable overlap with data available in literature.

This paper is organized as follow: section 2 describes the measurement object, focusing on the boundary conditions (2.1), the floor elements (2.2) and the mounting system (2.3). In section 3, the methods are introduced along with the specific experimental setup and the measurement program is presented (3.3). In section 4, we present and discuss the measurement results starting from the basic properties and then looking at the effect of specific factors on the sound radiation. In section 5, we briefly present how the observations of the radiated sound power can be interpreted in terms of impact noise level. Finally, in section 6, we present a summary of our findings. Two appendices address two questions related to the ITM method and its application on this specific setup. Appendix A presents the investigations related to the effect of the airborne excitation of the lower plate of the floor element. Appendix B presents the results showing that symmetry considerations cannot be exploited to reduce the measurement time when using the ITM method.

2. Measurement object

2.1. The WOODSOL building system (boundary conditions)

The Woodsol building system is a frame construction system with the following special features: 1) the frame is moment resisting in one direction, 2) the floor elements are of type *hollow box, 3)* the stiffness of the floor element is exploited in the frame structure to achieve moment resisting capacity.

The Woodsol frame is made of massive timber components, i.e. glulam columns. The principle is shown in the sketch in Fig. 1. In Fig. 2, we show the prototype of the system we built to perform several acoustic investigations, including part of the measurement presented in this paper.

In the prototype the columns were 5.2 m high and have a cross section with dimension 0.40 m × 0.45 m. The material used was glulam GL30c from Moelven. The floor elements were installed to the columns with the bottom flange 2 m above the laboratory floor. The columns were installed to the floor by means of a pin connection with the free rotational axis perpendicular to the floor element's longitudinal direction. This is also the direction where the frame is expected to be moment resisting. The columns were braced on top by means of aluminum profiles (not shown in the picture). In the prototype two floor elements shared the central columns. The floor elements were not connected to each other at any other point. In the following we will refer to the prototype setup as: "*on columns* boundary condition". This could be nearly considered as clamped at the corners, whereas this definition is not rigorous since a) the connection has a finite rotational stiffness [9] and b) the frame is moment resisting only around two axis, while the third one is undefined (i.e. rotation around one axis has no controlled constraints).

In order to understand the effect of the frame system on the modal and acoustical behavior of the floor elements, reference measurements with "*free-free* boundary conditions" were also performed. *Free-free* boundary conditions were achieved by installing the floor elements on air bellows (Figs. 3 and 4). One air bellow was placed at each corner of the floor element. The air bellows rested either on the floor of the lab or on massive blocks giving enough clearance (80 cm) to work under the floor element. The air bellows (Parker air bellows series 9109, type 6" × 1) were inflated to 6 bar giving natural frequencies for the rigid body motion at 3 Hz to 5 Hz. This was about 4 times lower than the first mode of the floor elements.

2.2. Floor elements

The investigated floor elements are of a hollow box type. The design used here is the optimized cross section, as described in [12] and shown in Fig. 5. The cross section has a total height of 0.5 m and was designed for a span length of 9 m to 10 m. We built

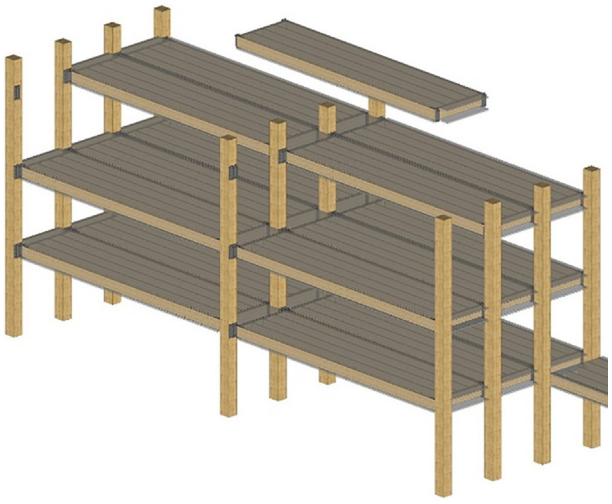

Fig. 1. Woodsol building system: frame construction based on moment resisting connection between continuous columns and stiff floor elements [11].

Fig. 2. Woodsol prototype; setup used for the on columns BC measurements, photo: SINTEF/A.-L. Bakken.

Fig. 3. Free-free boundary conditions: floor element installed on air bellows.

Fig. 4. Free-free boundary conditions: detail showing the air bellows.

prototype elements with lengths 9 m, 4.7 m and 3.7 m. All of them have the same cross section to ease the comparison of the results.

The top and bottom plates are laminated veneer lumber (LVL) panels with thickness 43 mm and 61 mm respectively. The outermost stringers are glulam GL30c, while the inner ones are glulam GL28c [11]. The materials properties are given in Table 1.

The top and bottom plates are glued to the stringers. Screws are used in the horizontal connections and are also used to ensure structural safety in vertical direction. A strong glued connection ensures no relative movements between components (composite effect $\gamma = 1$ to describe it according to Eurocode 5 [13]), while a screwed connection allows small relative movements ($0 < \gamma < 1$). In the Eurocode 5 [13] following relation is given, which describes how the composite effect affects the effective bending stiffness B_{eff}:

$$B_{eff} = \sum_{i=1}^{3} E_i I_i + \gamma_i E_i A_i a_i^2 \quad (1)$$

with E_i Young's modulus and I_i second moment of inertia of the i'th component in the cross section (e.g. i = 1 top plate, i = 2 vertical element, i = 3 bottom plate), A_i is the cross-sectional area of the i'th component and a_i is the distance of the component from the neutral axis.

To ensure full composite effect of the joint with the type of glue used, a line pressure between 0.6 N/mm^2 and 1.0 N/mm^2 is required [14]. The manufacturing process of the elements has been different for practical reasons and led probably to different composite effects in the three floor elements build. The two considered elements were built by two different groups of students in two different facilities, with different methods. During the gluing process of the 9 m element, the pressure was applied by means of screws. This ensures good control of the process and an applied line pressure close the required range. For the 4.7 m element, the pressure was applied by adding masses on top of the components to be glued. The resulting applied pressure is expected to have been as low as 0.01 N/mm^2.

In the work of Bjørge and Kristoffersen [12] the effective bending stiffness in longitudinal direction is determined analytically ($B_{L,\infty}$ = 1.6E8 Nm^2, $\gamma = 1$) and by means of deflection measurements on the 9 m element ($B_{L,eff}$ = 1.3E8 Nm^2, $\gamma = 0.75$). Based on the results presented in section 4.4, we estimated the longitudinal bending stiffness for the 4.7 m element as approximately $B_{4.7m,eff}$ = 6.4E7 Nm^2, $\gamma = 0.19$.

The cavity can be filled with gravel or absorbing material according to the acoustic requirements. We performed measurements with two configurations: empty element and cavity filled with 100 kg/m^2 gravel. The gravel was packed in bags to ease the installation (Fig. 6). The mass of the elements is given in Table 2.

2.3. Connectors

The WOODSOL connectors are designed aiming for a rotational stiffness in the range 8000 kNm/rad < K_θ < 13500 kNm/rad [9].

The connector is made by two metal parts. One metal part is fixed to the column, the other to the floor elements. Both are installed by means of threaded rods as shown in Fig. 7 [32]. The two metal parts are connected by friction bolts. The picture in Fig. 8 shows the current prototype version. Experimental investigations and improvement of the connection are ongoing.

3. Measurement methods and experimental setup

3.1. Experimental modal analysis (EMA)

3.1.1. EMA measurement principle

Experimental modal analysis (EMA) is a well-established measurement method. In the following we shall document the tools and the experimental setup used and highlight specific features. However, we will not present any background since this is outside

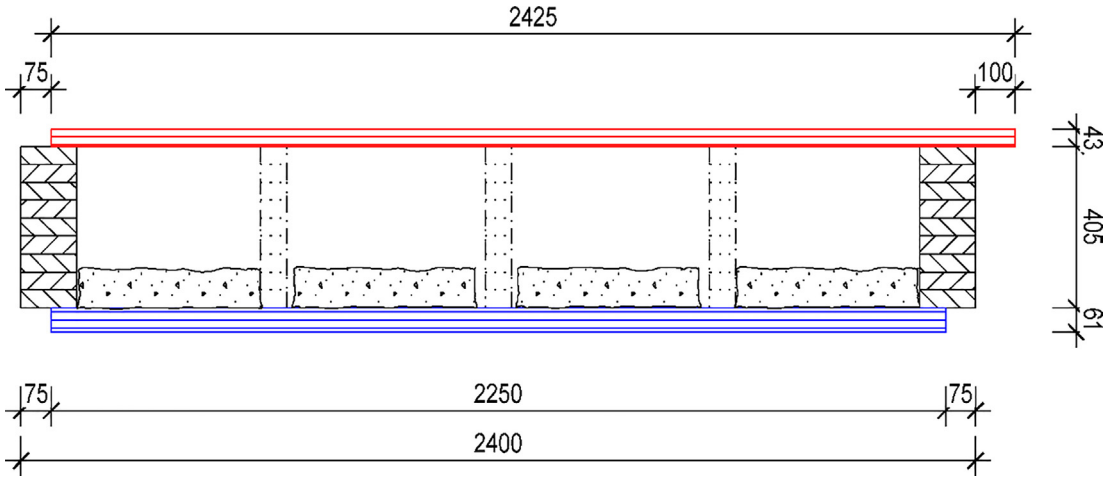

Fig. 5. Floor element cross section [11].

Table 1
Material parameters [12].

	ρ [kg/m3]	E1 [MPa]	E2 [MPa]	E3 [MPa]	G12 [MPa]	G13 [MPa]	G23 [MPa]	ν12	ν13	ν23
GL30c	430	13 000	300	300	650	650	65	0.02	0.02	0.30
LVL (Kerto-Q)	510	10 500	2 400	130	600	120	22	0.02	0.02	0.68

Fig. 6. Element cavity with the gravel bags.

Table 2
Weight of the elements and weigth of the added gravel.

Length	Timber weight (empty element)	Gravel (100 kg/m^2)
9.0 m	2400 kg	–
4.7 m	1300 kg	1200 kg
3.7 m	900 kg	900 kg

the scope of this paper, although literature is available on the subject [17,16].

The measurements were performed using the roving hammer technique with several reference accelerometers. The measurement procedure was based on 1) data acquisition using a multichannel acquisition system and 2) post-processing of the data (see Section 3.1.3).

3.1.2. EMA excitation and response acquisition

On the 9 m floor, a measurement grid with 10 × 5 points (size 0.56 m × 0.98 m) and 4 reference accelerometers were used. On the 4.7 m floor, a measurement grid with 9 × 5 points (size 0.55 m × 0.56 m) and 7 reference accelerometers were used. The measurement grid was aligned with the glulam beams and stringer. Both excitation and response acquisition were performed on the top side of the floor for practical reasons (Fig. 9a). This must be kept

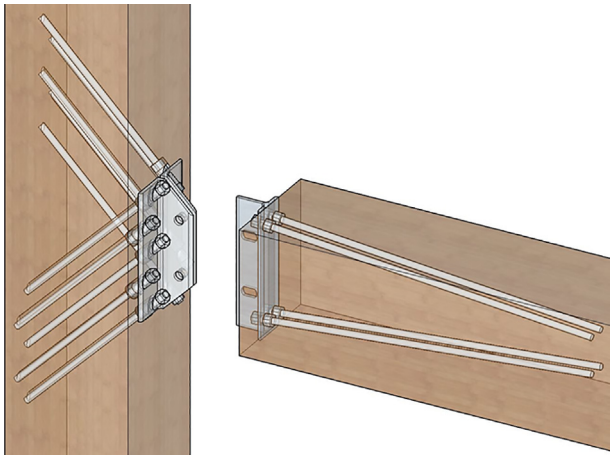

Fig. 7. Principle of the connector showing the threaded rods and the two connecting parts (graphic: A. Vilguts, NTNU).

in mind when comparing the results from the EMA measurements with the ITM results. At frequencies up to at least 100 Hz the vibrational behavior of the floor is dominated by the global modes (see section 4.1) and the upper and lower surface of the floor might be considered equivalent. With increasing frequency this assumption is not valid any longer, since local modes will behave differently on the top and lower surface.

An impact hammer with soft rubber cap was used to excite the structure. At least three impacts at each point of the grid were recorded as time signals using a multichannel acquisition system. The time between impacts was approximately 10 s allowing for enough window length to avoid leakage.

Excitation, response acquisition and analysis were limited to the vertical components.

3.1.3. EMA data analysis

The data were post processed using the Abravibe toolbox [15] in Matlab.

Fig. 8. Picture of the connector installed between the floor element and the column (photo: SINTEF/A.- L. Bakken).

The first step here was the impact processing. The optimal settings for triggering level, pretrigger, block size and windowing of both the force and acceleration signal were defined with help of the Abravibe toolbox graphical user interface. Then, the frequency response functions (FRF) were built by manually selecting the impacts to be used, based on visual check of the FRF and evaluation of the coherence function. The quality of the calculated FRFs was eventually checked by verifying the reciprocity of the FRFs at the reference points.

The poles and the modal participation factors were computed using the polireference time domain method (PTD). Based on the stabilization diagram, the reference positions that gave clearer mode functions were selected for the further steps. The Least Squares Frequency Domain (LSFD) method was used to estimate the mode shapes. The comparison between the measured FRF and those calculated by means of the extracted modal parameters is the first quality check. Moreover, the AutoMAC criterion was used to assess how well the identified modes are decoupled. Finally, the extracted mode shapes were checked visually for plausibility using the animation function of the toolbox.

3.2. Integral transform method (ITM)

3.2.1. ITM measurement principle

The integral transform method is based on the principle of a plane radiator as a sum of plane waves [17] and its theoretical formulation has been long used [18]. In recent years, it is gaining popularity thanks to the increasing availability of multichannel acquisition systems and scanning laser-vibrometers. We report here the main equations for ease of reference but otherwise refer to our previous paper for a compact overview of the method [19] or to the literature for more in depth insights [20–22].

The integral transform method is a hybrid method comprising of three main steps; 1) the measurement of vibration velocity on a relatively fine grid on the sound radiating surface, 2) a two-dimensional Fourier transform transforming the data in the wavenumber domain and 3) the calculation of the radiated sound power in the wavenumber domain using following equation [20]:

$$P[\gamma] = \frac{1}{2}\frac{\rho_A c_A}{4\pi^2}\mathrm{Re}\left[\sum_{\alpha=1}^{M_\alpha}\sum_{\beta=1}^{M_\beta}\mathbf{K}[\alpha,\beta,\gamma]\cdot\left|\hat{v}[\alpha,\beta,\gamma]\right|^2\Delta x^2\Delta y^2\right]\Delta k_x\Delta k_y \tag{2}$$

where: $\hat{v}[\alpha,\beta,\gamma]$ is the vibration velocity in the wavenumber domain, calculated by means of a 2D Fourier transformation for the coordinates α, β in the wavenumber domain at the frequency step γ. Δx and Δy is the distance between measurement points respectively in x and y direction, $M_\alpha = z_p\frac{l}{\Delta x}$ and $M_\beta = z_p\frac{b}{\Delta y}$ are the number of samples in the wavenumber domain, z_p is a zero padding factor required to achieve sufficient resolution, l and b are the dimensions of the plate, $\Delta k_x = \frac{2\pi}{z_p l}$ and $\Delta k_y = \frac{2\pi}{z_p b}$ are the sampling intervals in the wavenumber domain. The terms of the matrix **K** are:

$$\mathbf{K}[\alpha,\beta,\gamma] = \frac{k_A[\gamma]^2}{\sqrt{\left(k_A[\gamma]^2 - k_x[\alpha]^2 - k_y[\beta]^2\right)}} \tag{3}$$

where k_A is the wavenumber of the wave propagating in air, k_x and k_y are the wavenumber components in x and y direction of the waves propagating in the plate.

An advantage of the integral transform method is that the radiation efficiency σ follows directly from the equations above (adapted from [20]):

$$\sigma[\gamma] = \frac{\mathrm{Re}\left[\sum_{\alpha=1}^{M_\alpha}\sum_{\beta=1}^{M_\beta}K[\alpha,\beta,\gamma]\cdot\left|\hat{v}[\alpha,\beta,\gamma]\right|^2\Delta x^2\Delta y^2\right]}{\sum_{\alpha=1}^{M_\alpha}\sum_{\beta=1}^{M_\beta}\left|\hat{v}[\alpha,\beta,\gamma]\right|^2\Delta x^2\Delta y^2} \tag{4}$$

The use of the Fourier transformation and the finite size of the measurement object pose some limits of validity to the method, which are discussed in section 3.2.2.2 along with the chosen grid size.

3.2.2. ITM measurement setup

3.2.2.1. Installation of the test object. The test object was installed in an industrial hall as described in section 2.1. As is evident from Figs. 2 and 3, there were no partitions separating the volume above the floor element and the volume below. This raised two related questions: 1) can we apply the ITM method, which was originally developed for a baffled plane sound radiator? 2) How does the airborne excitation from the noise radiated by the upper part of the floor element affect the vibration velocity on the bottom of the element? We can apply the ITM method without a baffle only if the airborne excitation generates a vibration velocity at least 10 dB below the vibration velocity level generated by the direct impact excitation. We approached these issues experimentally by comparing the vibration velocity on the bottom plate generated by the tapping machine and by airborne excitation with comparable sound pressure level. The results show that if impact excitation is considered, the airborne excitation does not significantly affect the vibration velocity on the bottom plate and hence the ITM method can be applied. The details are presented in appendix A.

3.2.2.2. ITM measurement grid. The ITM method uses a 2-D Fourier transformation to convert the vibration velocity field from the space domain to the wavenumber domain. The Shannon criterion must be fulfilled in order to obtain valid results. This imposes a maximum measurement grid size as described by following equations:

$$\Delta x < \frac{\lambda_{x,min}}{2}, \quad \Delta y < \frac{\lambda_{y,min}}{2} \tag{5}$$

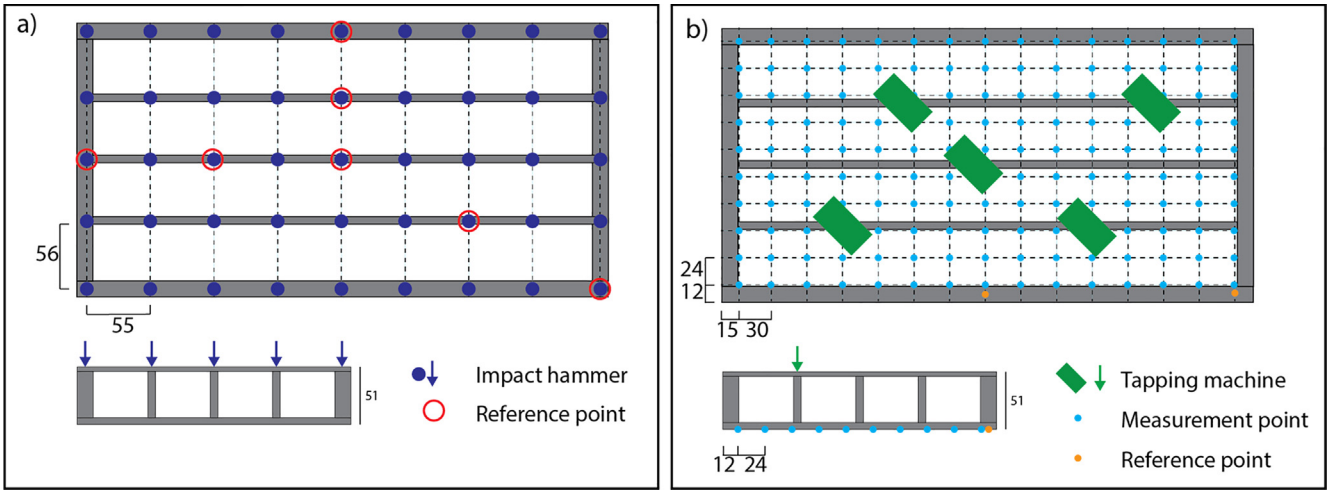

Fig. 9. a) EMA excitation and measurement positions, b) ITM excitation and measurement positions.

with $\lambda_{x,min}$ and $\lambda_{y,min}$ the wavelength in the plate at the highest frequency of interest. Since the relation between wavelengths λ_x, λ_y and frequency include the bending wave speed, and this is not readily known, there is an obvious challenge here. We opted for an educated guess by using plausible numbers and by comparing with existing literature values (see [19] for more details). In addition, after the first measurements were performed, we confirmed our assumptions by evaluating the bending wave speed from the wavenumber spectrum (see section 4.2, Fig. 12).

The resolution of the measurement in terms of wavenumbers is fixed by the dimensions of the measurement object. In our case:

$$\Delta k_x = \frac{2\pi}{l} = 1.33\frac{rad}{m}, \quad \Delta k_y = \frac{2\pi}{b} = 2.6\frac{rad}{m} \tag{6}$$

The use of zero padding is required in the numerical implementation to artificially increase the resolution [20].

We defined a measurement grid with 10 × 16 points with spacing 0.24 m × 0.30 m, giving following maximum wavenumbers within the Shannon criterium:

$$k_{max,x} = \pi/0.30\ \text{m} = 10.5\ \text{rad/m}$$
$$k_{max,y} = \pi/0.24\ \text{m} = 13.1\ \text{rad/m} \tag{7}$$

Looking at the dispersion relation after the measurements were performed (Section 4.2, Fig. 12), the frequency range where the measurements are valid can be established. We obtained following maximum frequencies:

$$f_{x,max} \cong 800Hz, \quad f_{y,max} \cong 500Hz \tag{8}$$

The weakest direction represents the theoretical limit of the method, in this case 500 Hz. However, it shall be noted that this theoretical limit might not be as strict depending on the specific radiation properties of the measurement object as discussed in [20].

The strong requirement on the grid size when using the Integral Transform Method to determine the radiated sound power leads to a high number of measurement points and hence to a long measurement time. One might argue that symmetry consideration could reduce significantly the measurement time and measurement costs. It is therefore important to verify if this concept could be applied. We performed our measurements on the 4.7 m elements covering the entire surface of the element. An investigation of the effect on the results produced by exploiting the symmetry was lightly verified by using different sets of the acquired data. The procedure and results are presented in appendix A. The results lead to the conclusion that symmetry cannot be exploited when using the ITM method. This confirms what suggested by [22] and proves wrong the assumption made by the author in [19]. These results also match the observations made by Hashimoto [23] while evaluating the Discrete Calculation Method (DCM), which share the same challenge as the ITM.

3.2.2.3. ITM excitation and response acquisition. In Fig. 9b, we show the excitation and measurement positions used for the ITM measurements.

The excitation was made by the ISO standard tapping machine positioned at five different locations on top of the floor element according to the requirement of the ISO16283 [10].

The vibration velocity was measured by integrating the acceleration signal measured by accelerometers. We used 12 accelerometers simultaneously. Two were kept fixed for phase reference and 10 were moved sequentially to cover all the rows of the measurement grid.

The acceleration was measured on the bottom of the floor element and only in the vertical direction, since this is the direction that dominates the sound radiation.

3.2.3. ITM procedure

For each configuration, the measurement procedure was as follows: 1) Excite at position one, 2) Record acceleration at row 1, 3) Move tapping machine to the next four positions, while recording the data at each position, 4) Move the accelerometers to the next row and repeat the steps 1 to 4.

The analysis was made in post processing. The radiated sound power was calculated individually for each excitation position and then averaged energetically as indicated in the standard.

3.3. Measurement program

The extensive measurement program shown in Table 3 was carried out to achieve the goals stated in the introduction. It includes several different configurations based on the three parameters: floor length, boundary conditions and additional mass. On each configuration, both an experimental modal analysis with a rowing hammer (EMA) and the measurement of the radiated sound power (ITM) under excitation by the tapping machine were performed.

Table 3
Measurement program. Some of the configurations were described in the given references.

Measurement	Floor length	Boundary conditions	Additional mass	Refs.
EMA, ITM[1]	9 m	free-free	no	[19,24]
EMA	9 m	clamped	no	[12]
EMA	9 m	simply supported	no	[12]
EMA, ITM	4.7 *m*	free-free	a) no b) gravel, 100 kg/m^2	
EMA, ITM	4.7 m	on columns	a) no b) gravel, 100 kg/m^2	
EMA, ITM	3.7 m	free-free	gravel, 100 kg/m^2	
EMA, ITM	3.7 m	on columns	gravel, 100 kg/m^2	

[1]) Data are available for only half of the floor element.

4. Measurement results

4.1. Frequency response functions and mode shapes

In this section, we present the general form of the recorded frequency response functions (FRF) and we establish the correspondence between the peaks in the FRF and the mode shapes. The respective natural frequencies and damping values are given in Table 4.

The diagrams in Fig. 10 show the FRFs magnitude measured on the 4.7 m floor element without additional mass mounted with free-free BC (upper diagram) and mounted on columns (lower dia-

Table 4
Natural frequency f and damping ζ of the identified modes on the 9 m and 4.7 m element with and without gravel installed with free-free BC and on columns BC. *) indicates uncertain data; -) indicates that the mode was not detected.

9 m element			4.7 m element								
Without gravel				Without gravel				With gravel			
free- free				free- free		on columns		free- free		on columns	
Mode	*f (Hz)*	*ζ (%)*	*Mode*	*f (Hz)*	*ζ (%)*	*f (Hz)*	*ζ (%)*	*f (Hz)*	*ζ (%)*	*f (Hz)*	*ζ (%)*
1st torsional	26.0	1.0	1st torsional	40.5	1.8	–	–	36.1	1.7	47.1	4.2
1st longitudinal	31.9	0.5	**1st transverse**	56.5	2.1	59.3	2.4	38.4	1.0	40.7	2.5
2nd torsional	42.1	0.8	2nd torsional	68.2	1.1	94.6	2.1	58.9*	3.6	–	–
1st transverse	42.7	1.0	**1st longitudinal**	81.3	1.2	101.3	1.7	57.3	1.8	64.0*	–
Antisymmetric	65.7	1.7	2nd transverse	85.0	1.1	81.3	1.8	48.5	1.5	54.5	4.9
2nd transverse	71.9	0.9	Antisymmetric	103.0	2.0	–	–	–	–	–	–
2nd longitudinal	72.3	1.7	3rd transverse	115.6	1.1	–	–	–	–	–	–
Higher order	75.0	0.8	Higher order	132.9	2.0	–	–	–	–	–	–
Higher order	95.5	0.8	Higher order	136.9	1.5	–	–	–	–	–	

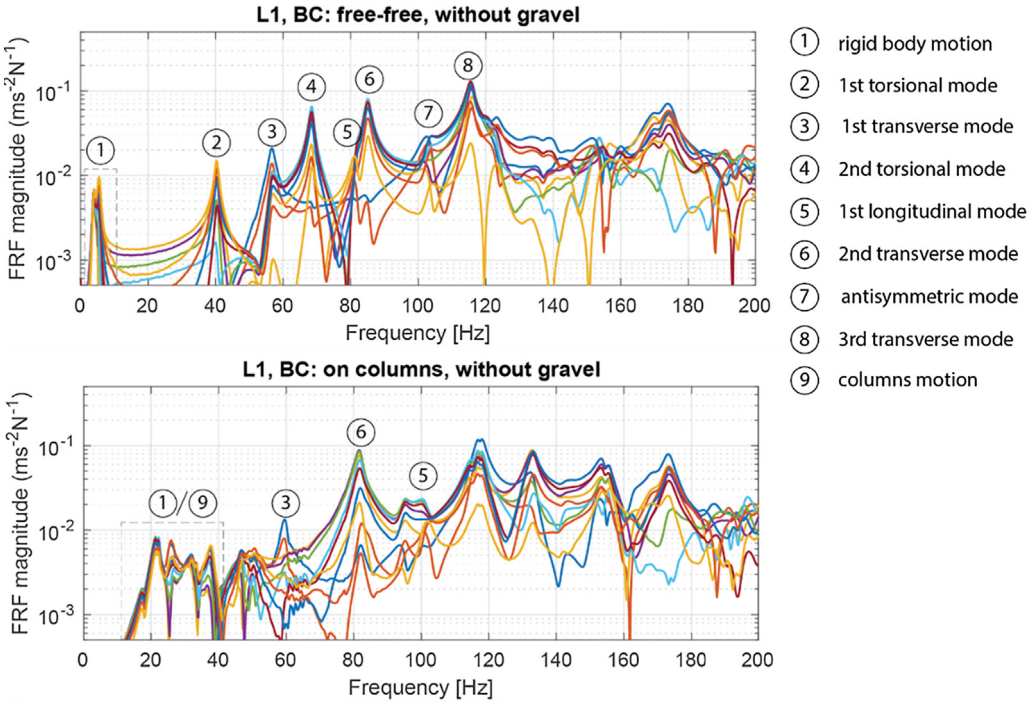

Fig. 10. Frequency response functions measured on the 4.7 m element without gravel showing the identified vibrational modes: the upper diagram presents the results obtained with free-free boundary conditions; the lower diagram presents the results obtained with element on columns.

gram). The numbers above the peaks of the FRFs identify the corresponding vibrational mode, which are graphically presented in Fig. 11. A detailed analysis and discussion of this data is presented in Section 4.3.

At this stage, we highlight the features indicated with the numbers 1 and 9. In the upper diagram, we recognize at least two main peaks, grouped under the number 1. They describe the motion of the floor as rigid body on the air bellows. In the lower diagram, the group of peaks at the frequencies between 20 Hz and 40 Hz is marked with the numbers 1/9. Some of the peaks here correspond to the vibrational modes of the prototype's columns while others describe the rigid body motion of the floor on the connectors. Even if the connectors present a high rotational stiffness, they exhibit a relatively soft behaviour in the vertical direction.

4.2. Bending waves dispersion curve

The diagram in Fig. 12 shows the vibration velocity wavenumber spectrum in the format k_x (longitudinal direction) versus frequency at $k_y = 0$, measured on the 4.7 m element on free-free boundary conditions, without additional mass. At each frequency step the amplitude was normalized to the maximum in the same frequency step. Data are shown in dB. The measurement resolution was $\Delta k = 1.34$ rad/m. The wavenumber spectrum was calculated using a zero padding factor $z_{pad} = 4$, corresponding to $\Delta k = 0.33$ r ad/m . The data are presented with a frequency resolution $\Delta f = 2$ Hz. The data is presented up to 800 Hz, since no major aliasing effects were observed up to this frequency and the extended frequency range helps assessing the trend.

In the diagram, two curves are overlaid to the measurements data. They were calculated using following relation based on the Mindlin thick plate theory (from [25] which cites [26,27]):

$$k_{B,eff} = 2\pi f \left(\frac{1}{2}\left(\frac{\rho h^3}{12B} + \frac{\rho}{\kappa G}\right) + \frac{1}{2}\sqrt{\left(\frac{\rho h^3}{12B} + \frac{\rho}{\kappa G}\right)^2 + 4\frac{\rho h}{B4\pi^2 f^2} - 4\frac{\rho^2 h^3}{12B\kappa G}} \right)^{\frac{1}{2}} \tag{9}$$

Following symbols and quantities were used: f frequency, ρ density of the material (here calculated as total volume divided by total weight), h height of the element, B bending stiffness, $\kappa = 0.9554$ [28], plate shear modulus $G = 6.5 \times 10^8$ Pa. The curve *"Element"* was calculated with the measured effective bending stiffness as given in Section 2.2. The curve *"Kerto"* was calculated using the Young's modulus of Kerto while the other parameters were left unchanged.

Despite the low resolution in the wavenumber spectrum, it seems appropriate to recognize three different regions: below 200 Hz the element shows a lumped behaviour as suggested by the curve *"Element"* fitting reasonably the measured wavenumber spectrum; above 500 Hz the wavenumber spectrum seems to be dominated by the LVL properties as suggested by the curve *"Kerto"* fitting with increasing agreement the measured data; in between there is a transition zone that do not follow the expected trend from the thick plate theory.

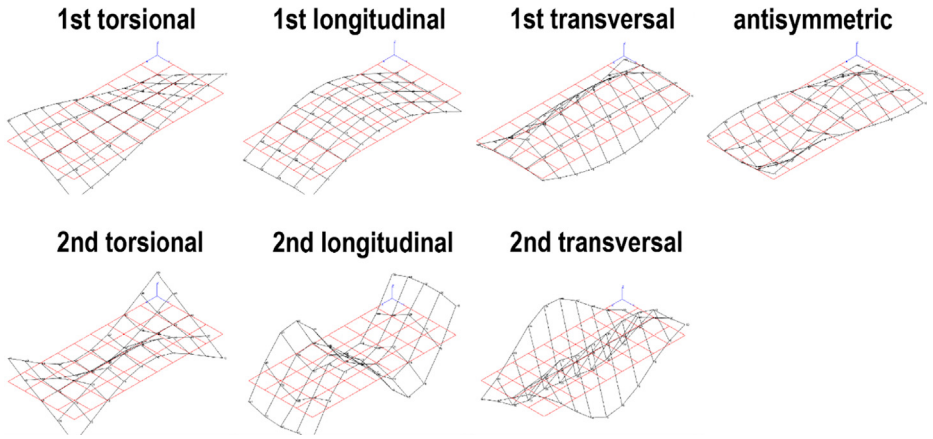

Fig. 11. Identified mode shapes. See Table 4 for the respective frequency and damping information.

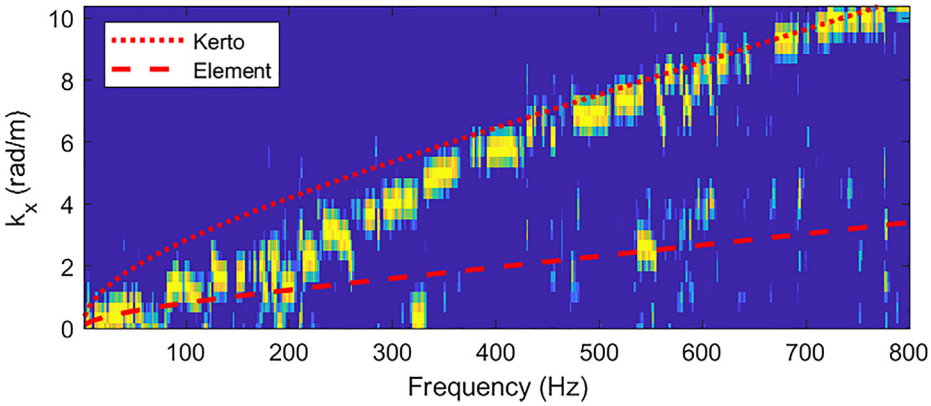

Fig. 12. Wavenumber spectrum of the measured vibration velocity plotted for $k_y = 0$, normalized to the maximum amplitude at each frequency step. Overlaid lines: see text.

4.3. Effect of boundary conditions

Fig. 13 presents a comparison of the frequency response functions (FRFs) measured with different boundary conditions: "free-free" and "on columns". The results are presented for the two configurations a) without additional mass and b) with additional mass (100 kg/m^2 gravel). In each diagram, only a selection of curves is presented, showing the FRFs with highest magnitude. The selection is kept constant among the diagrams. The natural frequencies for the identified modes are listed along with the damping for the two mounting conditions in Table 4.

Below we present a few observations based on the results presented in Fig. 13 and Table 4.

Transversal modes are nearly unaffected by the mounting on the columns (see also Fig. 10) while the amplitude of the torsional modes (e.g. 1st at 40 Hz and 2nd at 70 Hz) is dramatically reduced.

The natural frequency of the 1st longitudinal mode is shifted from 81 Hz (free-free) to 101 Hz (on columns) (see also Fig. 10). This result is surprising since 1) an ideally clamped beam would have the same natural frequency as with free-free boundary conditions and 2) all other support conditions would imply a lower natural frequency compared to free-free or clamped [17]. A possible explanation of the increased natural frequency is that the threaded rods reduce the effective length of the floor by extending the clamping fixture. The result here fits well with a reduction in length of the floor as high as 60 cm, which is the length of the inserted rods. It seems that the connections shift the supporting point approximately half way in the rods, corresponding to 30 cm on each side of the floor. If this result can be confirmed by further investigation, it would imply that a clamped support, as realized in this project, would have two beneficial effects on the achievable span. Firstly, by exploiting the difference between simply supported and clamped and secondly by reducing the effective length of the floor, hereby increasing the achievable span length with constant cross section or conversely allowing a reduction of the cross section for constant span.

Modal damping increases up to a factor of 2 on selected modes (2nd torsional mode).

Finally, above 125 Hz the effect of the boundary conditions is very limited.

Fig. 14 shows the corresponding radiated sound power, again for the two configurations a) without additional mass and b) with additional mass (100 kg/m^2 gravel). Each curve corresponds to the energy-averaged sound power level. The shaded area corresponds to ±σ, where σ is the standard deviation calculated between the measurements at the individual excitation positions.

The data presented in Fig. 14 show that the effect on the radiated sound power is limited to narrow frequency bands corresponding to the missing modes in that frequency band. Without gravel the effect is almost negligible between 40 and 400 Hz. With

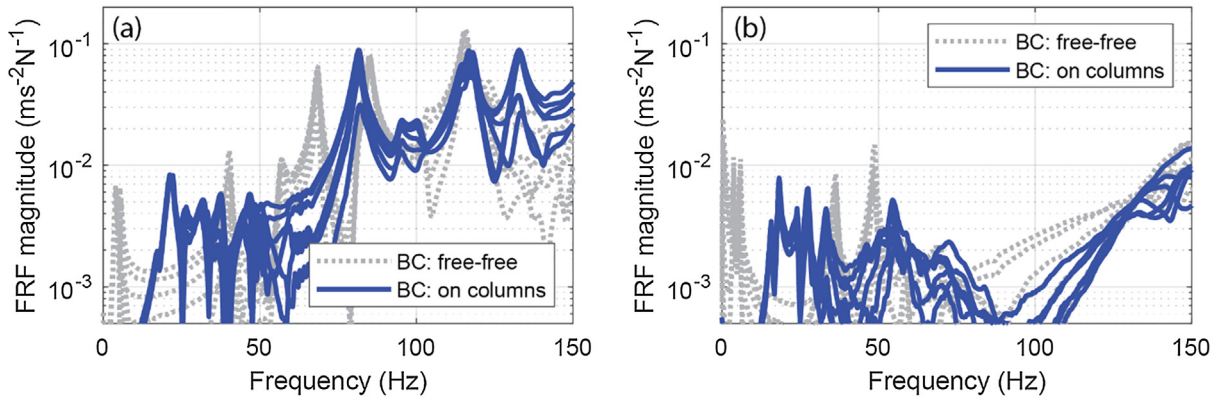

Fig. 13. Frequency response functions for the boundary conditions "free-free" and "on columns". (a) show the effect on empty elements, (b) show the effect on elements filled with 100 kg/m^2 gravel.

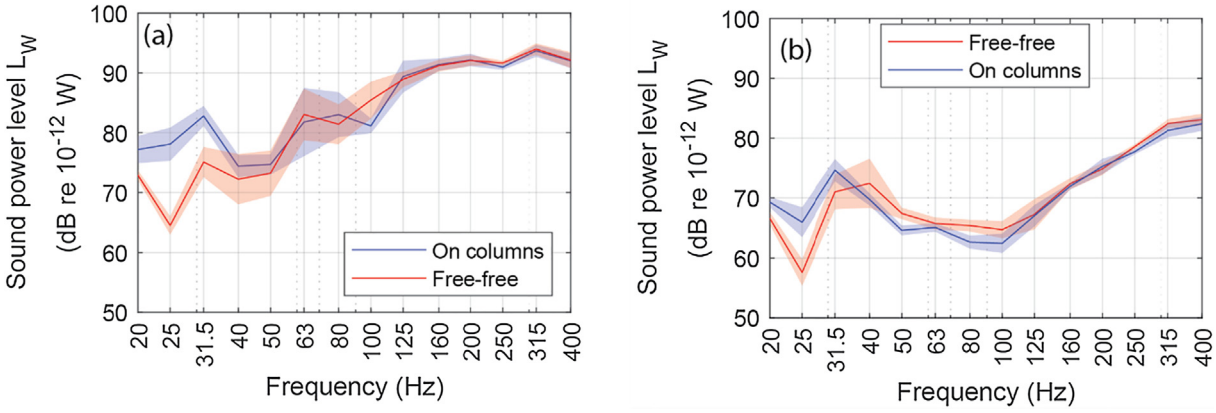

Fig. 14. Radiated sound power for the boundary conditions "free-free" and "on columns". (a) show the effect on elements without additional mass, (b) show the effect on elements with 100 km/m2 gravel as additional mass in the cavity.

gravel, the effect is up to 3 dB sound power reduction in the frequency range from 40 Hz to 100 Hz when mounting the element to the columns.

Below 40 Hz we observe a clear increase of radiated sound power when mounting the element on the columns. This is mainly related to vibrational modes on the undamped columns, which force vibrations on the floor element. It is to clarify if this effect will be also observed in real buildings, where the columns experience more constraints and possibly higher damping.

4.4. Size effect

We start assessing the size effect by looking at the recorded frequency response functions and the position of the identified modes. Fig. 15 shows a selection of the frequency response functions recorded respectively for the 9 m floor and 4.7 m floor (note that this is a subset of the data presented in Fig. 10). Table 4 shows the natural frequencies and damping of the identified modes.

The results in Fig. 15 and Table 4 give a clear indication of which parameters are mainly affected by the change in the length: longitudinal modes are clearly shifted towards higher frequencies when the length of the element is reduced. The frequency of transverse and torsional modes shifts towards higher frequency, by a factor 1.6 (3/4π). Since the transverse dimension was kept constant, this indicates that the structure stiffens in transversal direction by the effect of the end beams getting closer, when reducing the length of the element.

The shorter floor element experiences a slightly higher modal damping.

Fig. 16 shows the radiated sound power level L_w for the 9 m and the 4.7 m elements. Each curve corresponds to the energy-averaged sound power level. The shaded area corresponds to ± σ, where σ is the standard deviation, calculated between the measurements at the individual excitation positions. Note that these data are based on measurements performed on only half of the bottom surface. The reason for this is that the measurements on the 9 m element were performed at an early stage of the project and the vibration velocity was measured only on half the surface. As stated in section 3.2.2.2, symmetry cannot be exploited when using the ITM method. To keep the results comparable, the analysis has been performed using only half of the measurement surface for both the 9 m and the 4.7 m floor element. In this way, the absolute level of the radiated power is not correct at low frequencies but the comparison yields.

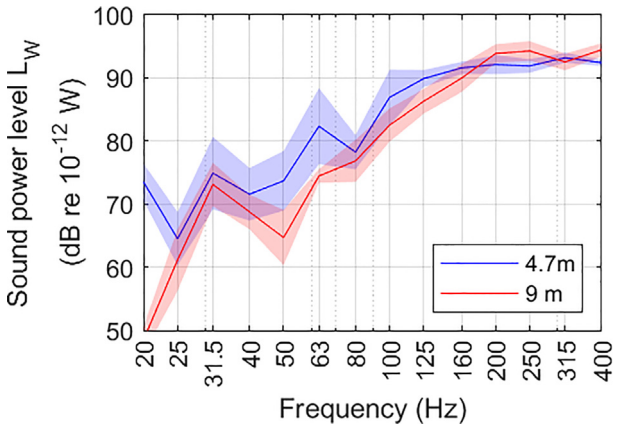

Fig. 16. Radiated sound power measured on the bottom surface of the 9 m and 4.7 m element. Both elements without gravel, BC: free-free. Note that these results are calculated using only half of the bottom surface.

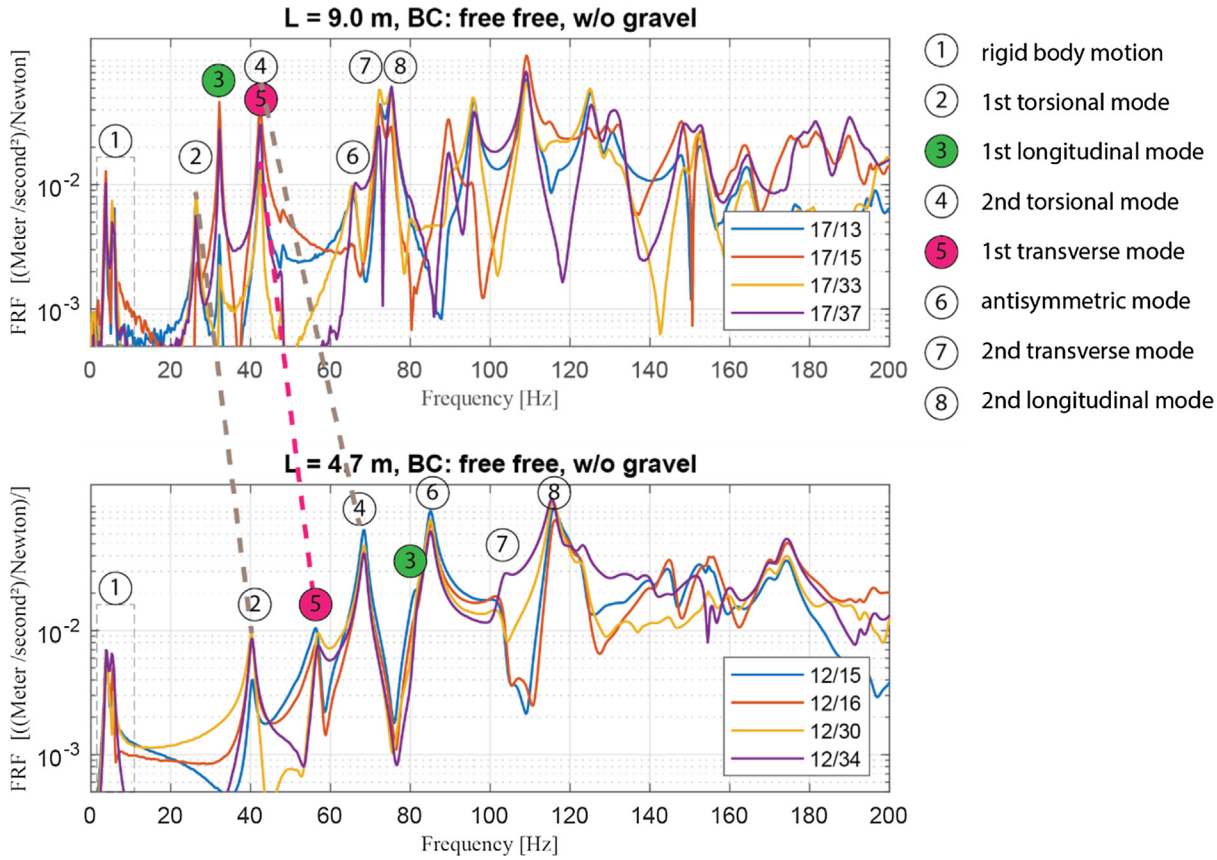

Fig. 15. Frequency response functions measured on the 4.7 m and 9 m element without gravel. The numbers mark the identified modes.

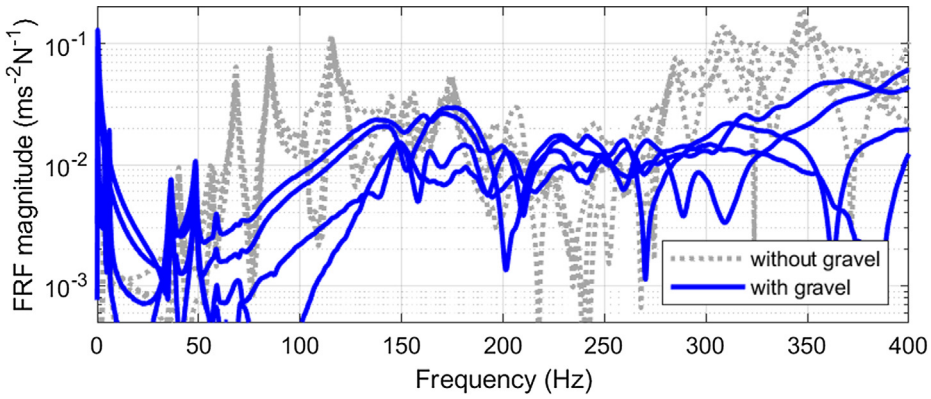

Fig. 17. Measured frequency response functions with the element installed with «free-free» boundary conditions. The frequency response functions measured with (100 kg/m^2) and without gravel in the element are compared.

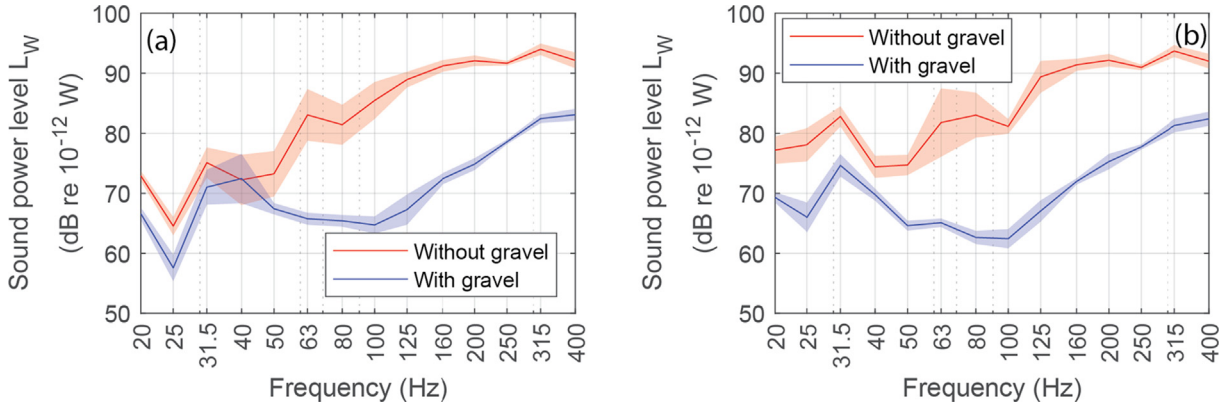

Fig. 18. Radiated sound power measured with and without gravel for the element mounted with (a) free-free BC and (b) "on columns".

Between 40 Hz and 80 Hz the overall L_w for the 4.7 m element is up to 10 dB higher than that for the 9 m element. This seems to relate well with the more even distribution of the vibrational modes in the 4.7 m elements. In the 9 m element there is indeed a clear gap in the FRFs from 43 Hz to 66 Hz.

4.5. Effect of gravel

The effect of additional mass (gravel) on the vibroacoustic behaviour of the floor element was observed best on the 4.7 m floor mounted with "free-free" boundary conditions. The results are presented in Fig. 17. The diagram shows the measured frequency response functions for selected response/excitation combinations with gravel (solid line) and without gravel (dotted line).

The effect of gravel is a strong attenuation of the vibrational modes above 50 Hz and a dramatic increase in damping.

The diagrams in Fig. 18 show the radiated sound power determined with the ITM method with and without gravel, both for free-free boundary conditions and for the floor element mounted on the columns. Each curve corresponds to the energy-averaged sound power level from the five tapping machine positions. The shaded area corresponds to ± σ, where σ is the standard deviation calculated between the measurements at the individual excitation positions.

The results show a reduction of the radiated sound power larger than 10 dB (up to 20 dB) above 50 Hz by adding 100 kg/m^2 gravel in the cavity of the floor elements. A reduction of 5 dB to 10 dB is observed also between 20 Hz and 50 Hz with a minimum at 40 Hz (0 dB with free-free BC), where the 1st torsional mode seems to be unaffected by the additional mass. In the "on columns" case, the increased damping and increased impedance of the floor seem to mitigate the forced vibrations generated by the columns.

5. Impact noise level

The results are presented in this paper in terms of radiated sound power L_w. However, the observed features and level differences can be directly interpreted in terms of impact noise level L_n. When the diffuse field assumption holds (i.e. above the Schroeder frequency), L_n can be calculated with this simple relation [29]:

$$L_n = L_w - 4\ \text{dB} \quad (10)$$

In typical acoustic laboratories for measuring impact noise level, this relation will hold above approximately 150 Hz.

Below the Schroeder frequency, the sound pressure level generated in the receiving room by the radiated sound power has first to be calculated considering the features of the sound field in the measuring room. Only then the impact noise level can be calculated. Roozen [30] investigated this topic, focusing on airborne sound insulation and the same approach could be used here. However, this will affect the absolute levels but not the differences obtained by changing the parameters. This means that the observed differences are directly valid also for the impact noise level.

6. Conclusions

We built a prototype of a building system based on long span hollow-box timber floor elements with moment resisting connec-

tors at the corners. The goal was to gain deeper knowledge of the vibroacoustic behaviour of the system. We performed several experimental investigations focusing on the modal behaviour of the floor elements and the radiated sound power under impact excitation. We used two techniques to obtain our results: experimental modal analysis and Integral transform method. This made it possible to investigate the correct boundary conditions and to show the effect of the size of the element on the measurement results.

Our overall conclusion is that the measured transfer functions and the standard deviation related to the excitation position lead to identify two frequency ranges: a lower one from 20 Hz to 150 Hz with isolated modes and large variance of the measured radiated sound power depending on the excitation position, and an upper one above 150 Hz where the modal density is higher, and the standard deviation is reduced from more than 5 dB to less than 2 dB. Both the effects related to the boundary conditions and those related to the size of the elements are more pronounced in the lower frequency range. Considering that the low frequency range is determining annoyance in wooden lightweight buildings [31], the obtained results are particularly important.

The studied boundary conditions affect the modal behaviour at frequencies below 125 Hz. The amplitude of torsional modes is dramatically reduced, and the natural frequencies of the longitudinal modes are shifted towards higher frequencies. The effect on the radiated sound power strongly depends on the modal distribution and on the modal properties. We observed a reduction of the radiated sound power up to 3 dB in the measurements on columns. This result highlights the need for representative boundary conditions when evaluating building elements in laboratory to achieve good reliability of the data at low frequencies. In our specific setup, the boundary conditions did not have a relevant effect on sound radiations above 125 Hz, since the vibration field was less affected by the boundary conditions with increasing frequency. This cut-off frequency might vary with varying boundary conditions.

The effect of size is mainly related to the distribution of the vibrational modes and reflects clearly in the radiated sound power. Surprisingly, the radiated sound power L_w for the shorter element exceeds L_w for the long element by up to 10 dB between 40 Hz and 80 Hz. Above 160 Hz the differences decrease significantly. This poses again a strong requirement on the element size when measuring the acoustic properties of long span element at low frequencies and highlights a shortcoming of standard acoustic laboratories.

The findings above show the importance of the recently developed advanced measurement methods to determine the acoustic properties of building components such as the ITM used for the measurements in this paper. The findings also show that measurements in standard acoustic laboratories might produce misleading results, when investigating stiff long span structures at low frequencies.

Regarding the effect of additional mass by means of gravel, the conclusion is that it has a dramatic effect on the radiated sound power, specially above 50 Hz, where we observed a reduction largely exceeding 10 dB over wide frequency ranges. For lower frequencies the effect is limited and some modes (e.g. the torsional ones) might not be affected at all by the additional mass.

Finally, the information presented in the appendix provide following important results: 1) the results obtained with this measurement method are not affect by the direct airborne excitation, when impact excitation is used and the hall volume is large enough to avoid excessive sound pressure levels, 2) symmetry cannot be exploited with ITM. Cancellations effects are not accounted for, leading to excessive radiated energy compared to a full measurement. This effect might be negligible in frequency ranges with high modal density, in our case above 160 Hz.

Declaration of Competing Interest

The authors declare that they have no known competing financial interests or personal relationships that could have appeared to influence the work reported in this paper.

Acknowledgments

This study has been carried out within the Woodsol project, a project funded by The Research Council of Norway and leaded by Kjell Arne Malo at NTNU. The project includes research at NTNU and SINTEF Building & Infrastructure and the PhD grant for the first author of this paper, which is gratefully acknowledged. Petra Rüther at SINTEF was work package leader for "WP6 Prototype", which made the prototype possible. Sveinung Nesheim and Aivars Vilguts, both PhD students at NTNU and member of the Woodsol project, were involved in the design and construction of the WOODSOL prototype. Leif Joar Lassesen and students from Charlottenlund Videregående skole in Trondheim (NO) greatly supported us during the construction of the prototype. Kate Layton Matthews provided language support.

Appendix A:. Airborne effect

We are performing sound radiation measurements based on acceleration measurements under tapping machine excitation without confining walls around the excited surface. One natural question that arises is: what is the vibration velocity level caused by the airborne excitation due to the airborne noise generated by the tapping machine itself and being radiated by the upper flange of the excited floor element? Does this affect the vibration velocity level generated directly by the structure-borne excitation?

We answered these questions using following experimental procedure: 1) we first excited the floor element using the tapping machine and measured a) the sound pressure level at 1 m distance, 45 degree elevation from the tapping machine at two positions and simultaneously measured the vibration velocity at 6 positions on the bottom side of the floor element. 3 positions were on the joists and 3 were in between joists. 2) We then calibrated the excitation signal of a half dodecahedron to match the sound pressure level when the dodecahedron was placed at the same position as the

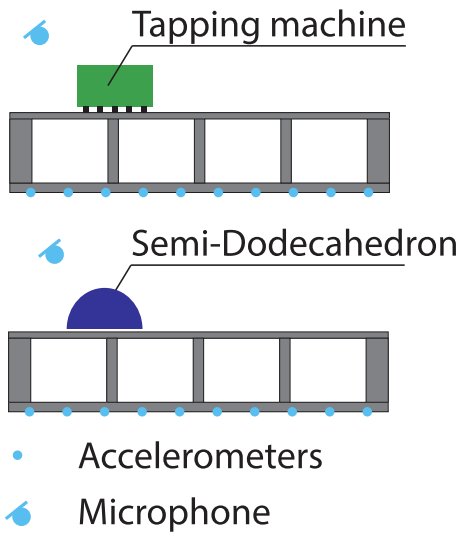

Fig. 19. Graphical representation of the procedure to assess the airborne effect.

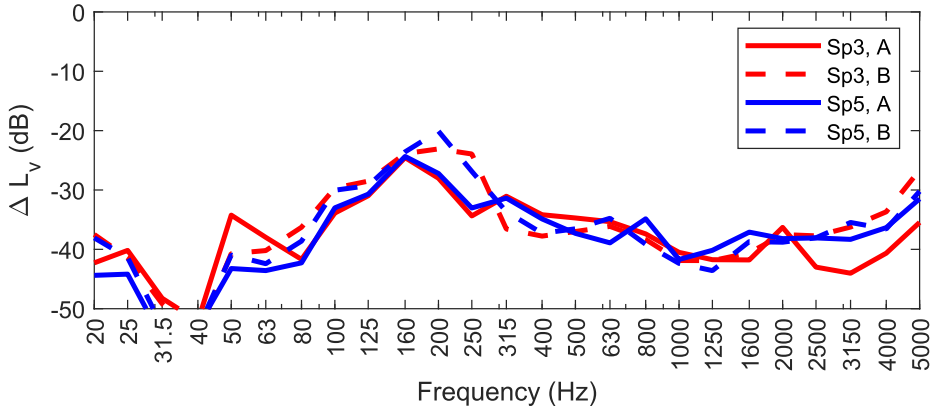

Fig. 20. Measured velocity level difference between excitation by tapping machine and excitation by loudspeaker.

tapping machine. The experimental setup is schematically shown in Fig. 19.

The dodechadron was installed using resilient material to avoid direct structure-borne excitation through the chassis. The vibration velocity on the bottom flange was then measured under the excitation of the calibrated loudspeaker. Finally, the vibration velocity level measured with structure-borne excitation was compared with the one measured with airborne excitation. The whole procedure was repeated for two excitation positions and two accelerometers groups.

In Fig. 20, we present the measurement results showing the effect of the airborne excitation. The curves show the difference between the vibration velocity level measured with airborne excitation by the loudspeaker and with tapping machine excitation. Four curves are presented, corresponding to two different excitation positions and the energetic average over two groups of accelerometers: group A with the accelerometers mounted on the joist, group B with the accelerometers mounted in between joists.

The measured data shows that the level difference is greater than −20 dB in the frequency range from 20 Hz to 5000 Hz. The minimum value of −20 dB is found in the 200 Hz one-third octave band and is probably related to the specific geometry and vibroacoustic properties of the specimen. We do not observe a significant trend related either to the excitation position or to the position of the accelerometers. A level difference greater than 10 dB ensures that the vibration level measured with tapping machine excitation is not affected by the airborne excitation. The safe margin that we found here allowed us to proceed without more detailed investigation. Nevertheless, we point out that this is not a general result and care should be taken whenever measurements are performed in smaller volumes (our hall had greater than 800 m^3) or with a limited height between the floor of the hall and the bottom side of the specimen. Other measurements we performed on a previous setup showed that with only 80 cm between laboratory floor and surface under test the velocity level difference is approaching −10 dB, smaller in some frequency ranges.

Appendix B:. ITM and symmetry

In this appendix we present the procedure that we followed to check if symmetry properties could be exploited when using the ITM method.

We calculated the radiated sound power and compared the respective results using following options:

a) All available data (full floor element),
b) Calculated radiated sound power based on only half data (in longitudinal direction) and add + 3 dB to the results to perform the comparison,
c) Build an artificial measurement data matrix from half the measured data by mirroring the data along the middle axis of the element,
d) Build an artificial measurement data matrix from half the measured data by mirroring the data along the centre point of the element.

The best results were obtained with strategy c) and are presented in Fig. 21.

Fig. 21 shows the radiated sound power level calculated using the measured vibration velocity over the full element (full) and calculated using the data for only half of the element (half) and strategy c). The results are almost identical above 50 Hz but a deviation of up to 6 dB is observed around the 31.5 Hz one-third octave band.

A possible explanation is that the effect relates to the first torsional mode. When measuring on full deck, two dipoles with opposite phase are observed and the effect of their interaction is accurately captured. When measuring only half deck the cancellation effect due to the phase relation cannot be captured and the energy is added rather than canceled.

These results lead to the conclusion that symmetry cannot be exploited when using the ITM method. However, in our case only minor deviations were observed above 50 Hz, suggesting that

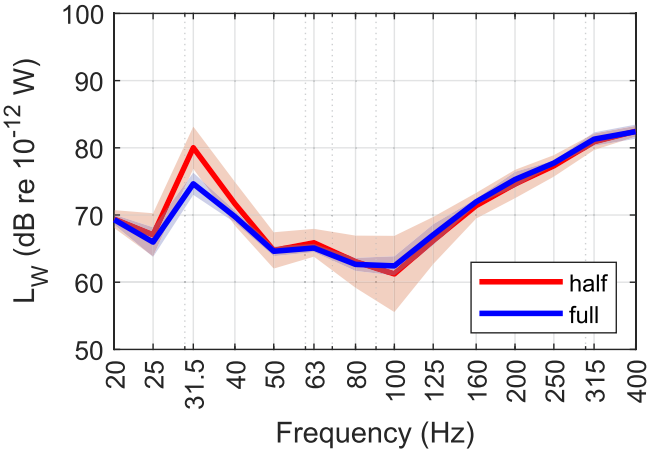

Fig. 21. Radiated sound power level calculated using the measured vibration velocity over the full element (full) and calculated using the data for only half of the element (half). Data source: 4.7 m element, with gravel, bc: on columns.

exploiting symmetry might be acceptable for higher frequencies, i.e. where the modal density is higher.

References

[1] Homb A, Guigou-Carter C, Rabold A. Impact sound insulation of cross-laminated timber/massive wood floor constructions: collection of laboratory measurements and result evaluation. Build Acoust 2017;24(1):35–52.
[2] Bartlomé O, Furrer B, Liebl A, Späh M, Kittel M. Acoustic developments in timber construction. In: Crocker MJ, editor. 21st International Congress on Sound and Vibration 2014 (ICSV 21) Beijing, China: International Institute of Acoustics and Vibration (IIAV); 2014.
[3] Melián Hernández A, Geyer C, Müller A, Pichler J, Sanavi A, editors. Direct and flanking airborne and impact sound insulation of different Swiss timber floor and wall constructions. Forum Acusticum; 2014; Krakow: European Acoustics Association (EAA).
[4] A. Homb Evaluering av lydegenskaper for bærende dekkekonstruksjoner, Woodsolo note no 01/17 2017 Trondheim.
[5] Skaar C, Solem B, Rüther P, editors. Composite floors in urban buildings: Options for a low carbon building de-sign. 6th Forum Wood Building Nordic Trondheim; 2017.
[6] StoraEnso. CLT rib panel brochure, www.storaenso.com, 11/2018.
[7] MetsäWood. Kerto-Ripa brochure 2019 [Available from: https://www.metsawood.com/global/Tools/MaterialArchive/MaterialArchive/Kerto-Ripa-Brochure-UK.pdf.
[8] Malo KA, Köhler J, Vibrations of timber floor beams with end restraints. Structures and Architecture: Concepts, Applications and Challenges–Proceedings of the 2nd International Conference on Structures and Architecture, ICSA; 2013. London: CRC Press.
[9] Vilguts A, Malo KA, Stamatopoulos H. Moment resisting frames and connections using threaded rods in beam–to-column timber joints. Seoul: WCTE; 2018.
[10] ISO16283-2:2018. Acoustics – Field measurement of sound insulation in buildings and of building elements – Part 2: Impact sound insulation.
[11] Halstedt H. Woodsol prototype element production drawings. Trondheim, NO: SINTEF Byggforsk; 2018.
[12] Bjorge V, Kristoffersen T. Konseptstudie av trebaserte kompositdekker med mulighet for innspenning til limtresoyler [Master Thesis]: NTNU; 2017.
[13] EN1995-1-1:2004. Eurocode 5: Design of timber structures - Part 1-1: General – Common rules and rules for buildings.
[14] Dynea. Technisches. Merkblatt für. Prefere 4094 2004.
[15] Brandt A. Notes On Using the ABRAVIBE Toolbox for Experimental Modal Analysis. In: http://www.abravibe.com, editor.
[16] Brandt A. Noise and vibration analysis: signal analysis and experimental procedures. John Wiley & Sons; 2011.
[17] Cremer L, Heckl M, Petersson BA. Structure-borne sound: structural vibrations and sound radiation at audio frequencies. Springer; 2005.
[18] Maidanik G. Response of Ribbed Panels to Reverberant Acoustic Fields. J Acoust Soc Am 1962;34(6):809–26.
[19] Conta S, Homb A. Challenges and limitations using the Integral Transform Method to obtain the impact noise level of timber floors. In: Association EA, editor. Euronoise 2018; Creta2018.
[20] Kohrmann M. Numerical Methods for the Vibro-Acoustic Assessment of Timber Floor Constructions [Dissertation]: Technische. Universität München; 2017.
[21] Schoenwald S, Vallely S, Tröbs H-M. Advanced methods to determine sound power radiated from planar structures. J Acoust Soc Am 2017;141(5):3713.
[22] Winter C. Messtechnische Untersuchung leichter Deckentragwerke im Wellenzahlbereich und Prognose der abgestrahlten Schallleistung [Master]. Technische Universität München; 2012.
[23] Hashimoto N. Measurement of sound radiation efficiency by the discrete calculation method. Appl Acoust 2001;62(4):429–46.
[24] Conta S. Experimental modal analysis on Woodsol prototype floor element. NTNU/SDU 2017.
[25] Winter C, Müller G. Frequency Dependent Modeling for the Prediction of the Sound Transmission in Timber Constructions; 2018.
[26] Mindlin RD. Influence of rotatory inertia and shear on flexural motions of isotropic, elastic plates. J appl Mech 1951;18:31–8.
[27] Cremer L, Heckl M. Körperschall: physikalische Grundlagen und technische. Anwendungen: Springer-Verlag; 1996.
[28] Santoni A, Schoenwald S, Van Damme B, Fausti P. Determination of the elastic and stiffness characteristics of cross-laminated timber plates from flexural wave velocity measurements. J Sound Vib 2017;400:387–401.
[29] Vigran TE. Building acoustics. CRC Press; 2014.
[30] Roozen NB, Labelle L, Rychtáriková M, Glorieux C. Determining radiated sound power of building structures by means of laser Doppler vibrometry. J Sound Vib 2015;346:81–99.
[31] Ljunggren F, Simmons C, Öqvist R. Correlation between sound insulation and occupants' perception – Proposal of alternative single number rating of impact sound, part II. Appl Acoust 2017;123:143–51.
[32] Malo KA, Stamatopoulos H. Connections with threaded rods in moment resisting frames. Proceedings of the World Conference on Timber Engineering (WCTE 2016) 2016.